

Article

Evaluating Consistency of Snow Water Equivalent Retrievals from Passive Microwave Sensors over the North Central U. S.: SSM/I vs. SSMIS and AMSR-E vs. AMSR2

Eunsang Cho *, Samuel E. Tuttle and Jennifer M. Jacobs

Department of Civil and Environmental Engineering, University of New Hampshire, Durham, NH 03824, USA; Samuel.Tuttle@unh.edu (S.E.T.); Jennifer.Jacobs@unh.edu (J.M.J.)

* Correspondence: ec1072@wildcats.unh.edu; Tel.: +1-603-501-8377

Academic Editors: Claudia Notarnicola, Deepak R. Mishra and Prasad Thenkabail

Received: 27 March 2017; Accepted: 6 May 2017; Published: 10 May 2017

Abstract: For four decades, satellite-based passive microwave sensors have provided valuable snow water equivalent (SWE) monitoring at a global scale. Before continuous long-term SWE records can be used for scientific or applied purposes, consistency of SWE measurements among different sensors is required. SWE retrievals from two passive sensors currently operating, the Special Sensor Microwave Imager Sounder (SSMIS) and the Advanced Microwave Scanning Radiometer 2 (AMSR2), have not been fully evaluated in comparison to each other and previous instruments. Here, we evaluated consistency between the Special Sensor Microwave/Imager (SSM/I) onboard the F13 Defense Meteorological Satellite Program (DMSP) and SSMIS onboard the F17 DMSP, from November 2002 to April 2011 using the Advanced Microwave Scanning Radiometer for Earth Observing System (AMSR-E) for continuity. Likewise, we evaluated consistency between AMSR-E and AMSR2 SWE retrievals from November 2007 to April 2016, using SSMIS for continuity. The analysis is conducted for 1176 watersheds in the North Central U.S. with consideration of difference among three snow classifications (Warm forest, Prairie, and Maritime). There are notable SWE differences between the SSM/I and SSMIS sensors in the Warm forest class, likely due to the different interpolation methods for brightness temperature (T_b) between the F13 SSM/I and F17 SSMIS sensors. The SWE differences between AMSR2 and AMSR-E are generally smaller than the differences between SSM/I and SSMIS SWE, based on time series comparisons and yearly mean bias. Finally, the spatial bias patterns between AMSR-E and AMSR2 versus SSMIS indicate sufficient spatial consistency to treat the AMSR-E and AMSR2 datasets as one continuous record. Our results provide useful information on systematic differences between recent satellite-based SWE retrievals and suggest subsequent studies to ensure reconciliation between different sensors in long-term SWE records.

Keywords: satellite remote sensing; microwave; AMSR2; AMSR-E; F13 SSM/I; F17 SSMIS; snow water equivalent

1. Introduction

Snow is a fundamental water resource for humans and ecosystems. About 80% of the arid western U.S. and central Asia depend heavily on snowmelt as a water supply [1–3]. The snow-covered areas are reduced seasonally from 45.2 to 1.9 million km² over the lands of the Northern Hemisphere [2]. Consequently, many regions, for example, the Great Plains in U.S. and high-altitude mountain areas of western China, have experienced serious floods as a result of spring snowmelt [4–6]. Accurate estimates of snow water equivalent (SWE) are required to improve the capability of flood forecasting as a result of snowmelt, as well as water supply management [7,8].

Passive microwave sensors have proven to be valuable for monitoring snowpack distributions at global and regional scales because of a wide swath, the ability to operate day or night even under cloud conditions, and a response to the presence of snow at multiple frequencies [9]. Since November 1978, satellite passive microwave data from the Scanning Multichannel Microwave Radiometer (SMMR) aboard the National Aeronautics and Space Administration (NASA) Nimbus-7 satellite, and the Special Sensor Microwave/Imager (SSM/I) and Special Sensor Microwave Imager Sounder (SSMIS) aboard the Defense Meteorological Satellite Program (DMSP) series of satellites have been used for the SWE retrievals. The SMMR and SSM/I sensors have proven to be reliable passive microwave sensors and have been widely used for observing land surface conditions such as SWE [10–13], soil moisture [14,15], snowmelt [16–19], sea ice concentration [20,21], and freeze/thaw state [22,23]. Along with these instruments, the Advanced Microwave Scanning Radiometer for Earth Observing System (AMSR-E) on board the NASA Aqua satellite has successfully provided snow scientists and hydrologists with estimates of SWE from June 2002 to October 2011 [24–26]. Unfortunately, AMSR-E stopped operation in October 2011 due to a problem with its antenna. As a continuation of the legacy of AMSR-E, the Advanced Microwave Scanning Radiometer 2 (AMSR2) was launched in May 2012, onboard the Global Change Observation Mission 1-Water (GCOM-W1) satellite by the Japan Aerospace Exploration Agency (JAXA). With similar basic characteristics as AMSR-E, AMSR2 has provided geophysical datasets, including SWE and snow depth, retrieved by brightness temperature (T_b) measurements [27,28].

Although historical satellite sensors have provided SWE retrievals for about 40 years, the utility of continuous long-term SWE records depends on the consistency of measurements from different satellites over many years. For the SMMR and SSM/I sensors, there are several earlier studies dealing with similar topics. Armstrong & Brodzik [29] found 6 and 1 K differences between SMMR and SSM/I in the snow depth algorithm in the T_{b_{H19GHz}} and T_{b_{H37GHz}} channels, respectively. They suggested a modified snow depth equation to offset these differences. Derksen & Walker [10] identified a systematic T_b bias between the two sensors. They found that the T_b difference was dependent on magnitude of brightness temperature and overpass timing. Derksen et al. [30] demonstrated that the SMMR sensor notably underestimated SWE compared to SSM/I SWE, due to the instrumental differences. However, there are few studies for recent satellite sensors between continuous F13 SSM/I and F17 SSMIS and between AMSR-E and AMSR2 SWE retrievals, except for T_b calibration studies [31,32] and other variables [33]. This is likely because there is very little temporal overlap for the AMSR-E & AMSR2 and SSM/I & SSMIS (one year), making it nearly impossible to directly compare between the pairs of sufficient SWE data. In order to overcome this obstacle, we propose a cross-evaluation of consistency in the two time series, SSM/I-SSMIS and AMSR-E-AMSR2 SWE, using the relative SWE biases between the two time series. The SSM/I and SSMIS SWE are evaluated relative to AMSR-E SWE, AMSR-E and AMSR2 SWE are evaluated using the SSMIS SWE dataset.

This study focuses on the weekly maximum SSM/I (2002–2005), SSMIS (2007–2015), AMSR-E (2002–2010) and AMSR2 (2012–2015) SWE estimates over 13 winter seasons in 1176 watersheds in the North Central U.S. The paper is organized as follows. Section 2 describes the study region (North Central regions of the U.S.) focusing on topographical and climatic characteristics. Section 3 introduces the AMSR-E, AMSR2, SSM/I and SSMIS satellite SWE estimates including algorithms used in this work and their pre-processing. Section 4 describes the methodology used to evaluate temporal and spatial continuity in pairs of satellite-based SWE time series. Section 5 details the results and discussion of the comparative analyses between F13 SSM/I and F17 SSMIS SWE and between AMSR-E & AMSR2 SWE. Section 6 offers a summary and concluding remarks.

2. Study Area

The North Central region of the U.S. would benefit from a long-term record of satellite-based SWE estimates, because this area is vulnerable to frequent snowmelt floods [4,5,34,35] but has few snow observations [36]. Past studies have indicated positive trends in precipitation, runoff, and flood peaks

in the region, especially in the Red River of the North, potentially due to climate change [37,38]. The study area covers approximately 339,000 square miles including the U.S. portion of the Red River of the North, the Rainy River in Minnesota, and the Mississippi River from the upper region in Minnesota to Illinois, excluding the Missouri River basin (see Figure 1). Most of this region has a continental climate, which is characterized by temperature extremes. The prevailing weather systems come from the Gulf of Mexico in the summer and the dry Canadian air causes extremely cold temperatures in the winter. The warmest mean temperatures are in southern Iowa and Missouri with the coldest in northern Minnesota and North Dakota. Annual precipitation ranges from 356 mm in North Dakota to 1220 mm in Missouri. The precipitation occurs mainly during the summer season. Snowfall is the greatest in the Upper Peninsula of Michigan (up to 516 cm) and decreases away from the Great Lakes (e.g., North Dakota: 131 cm, Missouri: 56 cm). Average annual temperatures range from 4.7 to 12.5 °C and average temperatures during winter range from −11.0 °C in North Dakota to 0.2 °C in Missouri.

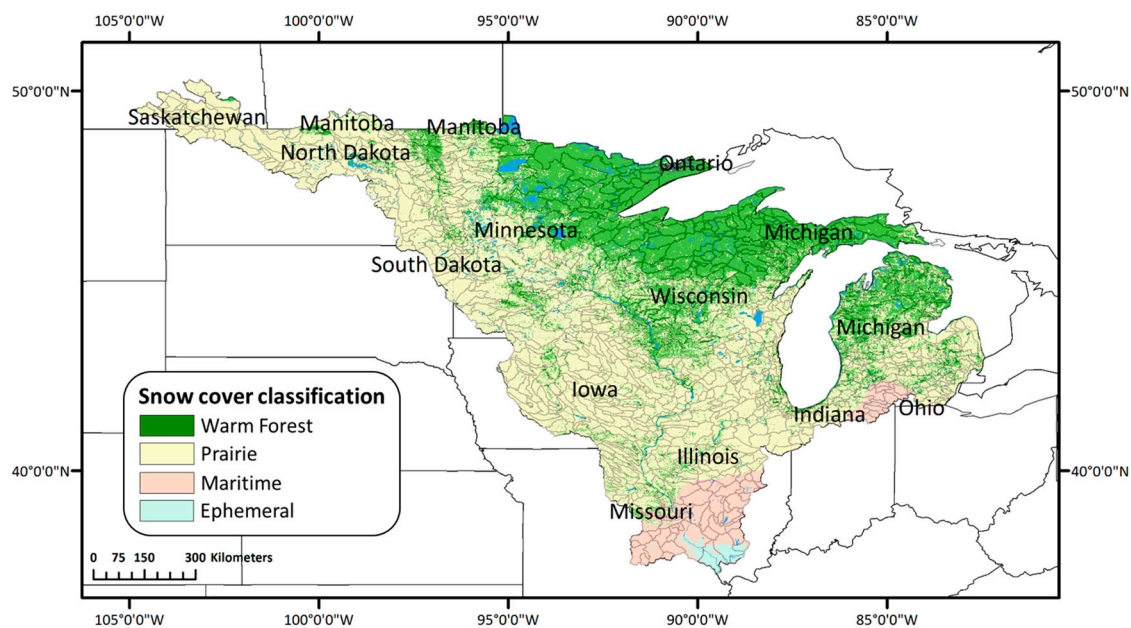


Figure 1. Overview map of the study region in the North Central U.S. with 1176 watersheds outlined and overlain snow cover classification.

Most of the U.S. North Central region's topography was formed by glacial processes. The eastern part of North Dakota and northwestern part of Minnesota are very flat, formed from glacial lake sediments, with mostly agricultural areas. The northern portion of Minnesota has forests and numerous lakes. The southern part is largely agricultural land with grass prairie and broadleaf forest. In Iowa, the topography is mainly rolling prairie with small changes in elevation, but the northeastern part of the state has rugged terrain. Illinois has little relief except for several mountains in the southern part. The topography of Wisconsin has forested areas with higher elevation and many glacial lakes in the northern part. The upper peninsula of Michigan is swampy in the east and relatively rugged in the upper west side, and the lower peninsula has gentle hills in the west.

In order to consider major spatial characteristics related to SWE estimates, the study region's 1176 National Oceanic and Atmospheric Administration North Central River Forecast Center (NOAA NCRFC) watersheds were divided into three major snow classes, Warm forest, Prairie, and Maritime using a seasonal snow classification system [39]. The Warm forest class covers northeastern Minnesota, Wisconsin, and Michigan and the Prairie class ranges over North and South Dakota, Iowa, southern Wisconsin, northern Illinois, and some parts of Missouri and Indiana. The southern parts of Missouri and Illinois and northern Indiana are classified as Maritime (Figure 1). The global snow classification system for seasonal snow cover has eight classes: Tundra, Taiga, Warm forest,

Prairie, Maritime, Ephemeral, Ice, and Water, expressed on the 1-km by 1-km spatial grid [39,40]. Each snow class was defined by an ensemble of snow stratigraphic characteristics including snow density, grain size, and morphologic crystal which is estimated from three climate variables: winter wind, precipitation, and air temperature [41]. Each of the watersheds over the study area was assigned a dominant snow class using the majority filter in ArcGIS. The warm forest, Prairies, and Maritime classes occupy 305, 767, and 67 watersheds, respectively.

3. Data and Preprocessing

3.1. SSM/I and SSMIS SWE

The series of SSM/I and SSMIS instruments onboard the Defense Meteorological Satellite Program (DMSP) platform series has provided continuous Tb measurements since July 1987. Among the SSM/I and SSMIS series, the F13 SSM/I and F17 SSMIS sensors provided Tb measurements from May 1995 to December 2007 (Data Version 1) and from December 2006 to present (Data Version 2), respectively [42]. Overpasses occurred at 7:00 a.m./p.m. for respective descending and ascending orbital nodes. In order to match the temporal ranges of the AMSR-E and AMSR2 (November 2002 to April 2016), we used continuous EASE-Grid Tb measurements, from the F13 SSM/I (November 2002 to December 2006) and F17 SSMIS (January 2007 to April 2016) sensors [43].

We then calculated daily SSM/I & SSMIS SWE estimates from Tb measured at the 19 and 37 GHz frequencies, using the Chang algorithm [44] as follows:

$$SWE = c(Tb_{H19GHz} - Tb_{H37GHz}) \quad (1)$$

where *SWE* is the snow water equivalent in mm; *c* is given as 4.8 mm/K [13,45]; Tb is the brightness temperature at different frequencies (19 and 37 GHz horizontal polarization). Only Tb measurements from the 6:00 a.m. descending overpass were used in order to reduce potential error by wet snow in the daytime [46].

3.2. AMSR2 and AMSR-E SWE

AMSR2 is a relatively new passive microwave sensor that is the follow-on instrument to its predecessor, AMSR-E [47]. The main improvements of AMSR2 compared with AMSR-E are a larger antenna (2.0 m diameter c.f. 1.6 m of AMSR-E) for enhanced spatial resolution, additional channels at C-band (7.3 GHz) for mitigating radio frequency interference (RFI), an improved calibration system, and an additional momentum wheel [32,47]. As a part of the afternoon-train (A-train) constellation of polar orbiting, Earth observing satellites, AMSR2 provides daily scans at approximately 1:30 a.m./p.m. local time at 1–2 days revisit time, beginning in May 2012. The most recent Level 3 AMSR2 SWE (Version 2.1) products, expressed on the same regular $1/4^\circ \times 1/4^\circ$ spatial grid, were acquired from the JAXA GCOM-W1 Data providing service (<http://gcom-w1.jaxa.jp>). The AMSR-E sensor onboard the Aqua satellite provided SWE retrievals at 1:30 a.m./p.m. local time from June 2002 to October 2011. Level 3 AMSR-E SWE data, expressed on the Equal-Area Scalable Earth Grid (EASE-Grid), were obtained from the National Snow and Ice Data Center [48].

Both the AMSR-E and AMSR2 SWE products were calculated based on the difference in brightness temperatures measured at 19.7 and 36.5 GHz along with some higher and lower frequencies. The SWE estimates were processed using the Kelly snow depth (SD) algorithm [25].

$$SD = ff(SD_f) + (1 - ff) \cdot (SD_0) \quad (2)$$

$$SD_f = 1 / \log_{10}(pol_{36GHz}) \cdot \frac{(Tb_{V18.7GHz} - Tb_{V36.5GHz})}{(1 - fd \cdot 0.6)} \quad (3)$$

$$SD_f = 1 / \log_{10}(pol_{36GHz}) \cdot \frac{(Tb_{V18.7GHz} - Tb_{V36.5GHz})}{(1 - fd \cdot 0.6)} \quad (4)$$

where SD is snow depth (cm), SD_f and SD_0 is the snow depth for forested and nonforested area, respectively, ff is forest fraction, and fd is forest density. The $pol_{36.5\text{GHz}}$ and $pol_{18.7\text{GHz}}$ are dynamic coefficients computed as the polarization differences at 36.5 and 18.7 GHz, respectively. The SD is converted to SWE by multiplying by the snow density for different snow classes based on the seasonal snow classification system in Sturm et al. [41].

The most recent AMSR2 SWE algorithm was updated to use forest transmissivity to improve the forest correction effect and false snow depth detections were flagged over the Tibetan Plateau region [28,49]. In order to minimize the wet snow impacts, this study used only descending SWE data, which were measured in the colder night time (01:30 a.m.) [46].

4. Methods

All available gridded daily SWE data from the two combinations of microwave sensors (AMSR-E & AMSR2 and SSM/I & SSMIS) were obtained for twelve winters from November 2002 to April 2016. For each of the two combination data sets, the gridded daily SWE were spatially averaged within each NCRFC watershed (1176 total in the study area). The data from AMSR-E and AMSR2 pixels near water bodies were flagged and removed, as were the negative SSM/I and SSMIS SWE values. Daily values were only calculated for watersheds with no missing data. For this work, a snow year runs from November to April labeled using the winter year. For example, the 2002 snow year means the period from November 2002 to April 2003.

Weekly SWE time series were produced for each watershed using the weekly maximum daily average SWE values to resolve the limitations of the satellite revisit times, which result in some days with no observations as well as low SWE values due to wet snow [13]. The weekly maximum SWE data were only calculated until the annual maximum SWE value within each winter year, to minimize uncertainties caused by late winter snow melting/refreezing cycles.

We consider two approaches to evaluate the satellite SWE estimates. First, we quantify the differences between AMSR-E and AMSR2 as well as SSM/I and SSMIS SWE data using conventional metrics, namely the coefficient of determination (R^2) and mean bias error (hereafter Bias):

$$R^2 = 1 - \frac{\sum (SWE_{AMSR-E\ or\ 2} - SWE_{SSM/I\ or\ IS})^2}{\sum (SWE_{SSM/I\ or\ IS} - \overline{SWE_{SSM/I\ or\ IS}})^2} \quad (5)$$

$$Bias_{original} = \sum (SWE_{AMSR-E\ or\ 2} - SWE_{SSM/I\ or\ IS}) / N \quad (6)$$

where $SWE_{AMSR-E\ or\ 2}$ is either the AMSR-E or AMSR2 SWE data, and $SWE_{SSM/I\ or\ IS}$ is either the SSM/I or SSMIS SWE data as the reference. $\overline{SWE_{SSM/I\ or\ IS}}$ is the mean SWE value for each watershed and N is the number of watersheds in each snow class.

Second, we compare yearly spatial bias maps between AMSR-E and AMSR2 with SSMIS SWE. Normalized bias is calculated using a normalization equation:

$$Bias_{normalized} = \frac{Bias_{original} - \overline{mean(Bias)}}{\overline{std(Bias)}} \quad (7)$$

where $Bias_{normalized}$ is the normalized bias and $Bias_{original}$ is the original bias between AMSR-E (AMSR2) and SSMIS SWE at each watershed. $\overline{mean(Bias)}$ is the total average of yearly mean bias and $\overline{std(Bias)}$ is the total average of yearly standard deviation of bias for the AMSR-E (2007–2010) or AMSR2 (2012–2015) period.

5. Results and Discussions

5.1. Comparison between SSM/I and SSMIS SWE

Temporal patterns between F13 SSM/I (2002 to 2005, four winters) and F17 SSMIS (2007 to 2010, four winters) were compared, using AMSR-E SWE as a baseline. The SSM/I and SSMIS SWE data in 2006 are not considered because the data are composed of F13 SSM/I SWE (November to December) and F17 SSMIS SWE (January to April). Figure 2 displays the three snow class averaged SWE time series according to snow classification.

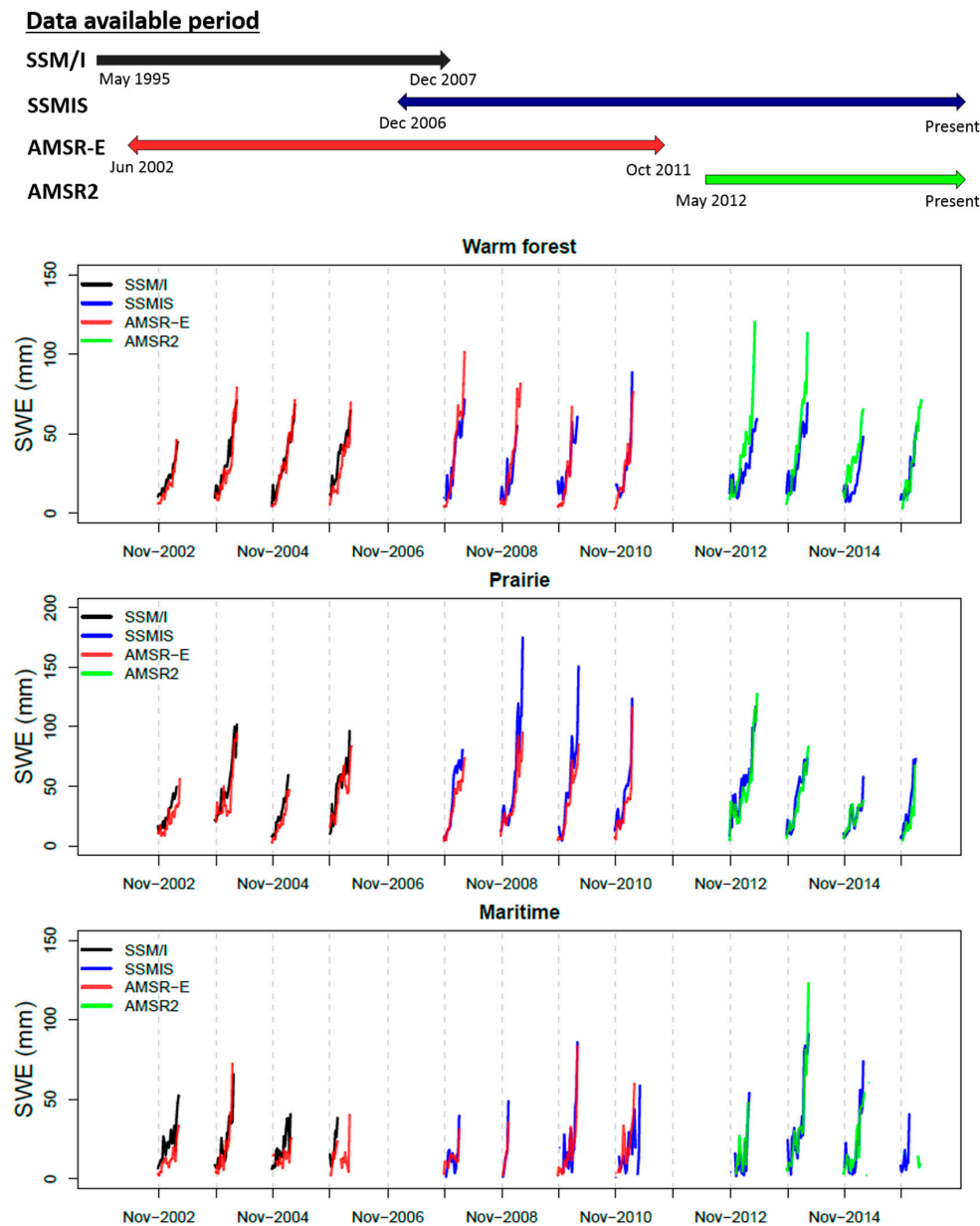


Figure 2. Date for which data are available by sensor and time series of weekly maximum snow water equivalent (SWE) from the Special Sensor Microwave/Imager (SSM/I) (blue), the Special Sensor Microwave Imager Sounder (SSMIS) (cyan), the Advanced Microwave Scanning Radiometer for Earth Observing System (AMSR-E) (black), and the Advanced Microwave Scanning Radiometer 2 (AMSR2) (red), according to snow classifications.

Temporal SWE variations are different among the three snow classes. Generally, the SWE time series in the Warm forest and Prairie classes show relatively clear temporal patterns with gradual increases throughout the winter and rapid decreases after maximum SWE values, while SWE time series in the Maritime have irregular temporal patterns. This variability could be related to characteristics of the Maritime snow class. This class was defined as warm deep snow with high air temperature and high precipitation and had the largest range in snow depth and density [39,41]. These characteristics could be due to snow melting/refreezing, resulting in difficulty in estimating SWE using Tb from passive microwave sensors. Another possible reason is that the snow class-averaged time series might not be representative of the temporal patterns of each Maritime watershed because there are relatively few watersheds in the Maritime class within the study area (5.7% of watersheds) and they are divided into two parts (southern Illinois and northern Indiana) in Figure 1.

For both the Warm forest and Prairie classes, increasing patterns of the SSM/I SWE throughout each winter generally correspond with AMSR-E SWE from 2002 to 2005. However, there are clear bias differences between the two classes in the SSMIS period (2007 to 2010). While the SSMIS SWE is lower than the AMSR-E in Warm forest, the SSMIS sensor overestimates SWE compared to AMSR-E in the Prairie in the middle of each winter season. The patterns are also evident in yearly bias between AMSR-E and SSMIS SWE in Figure 3.

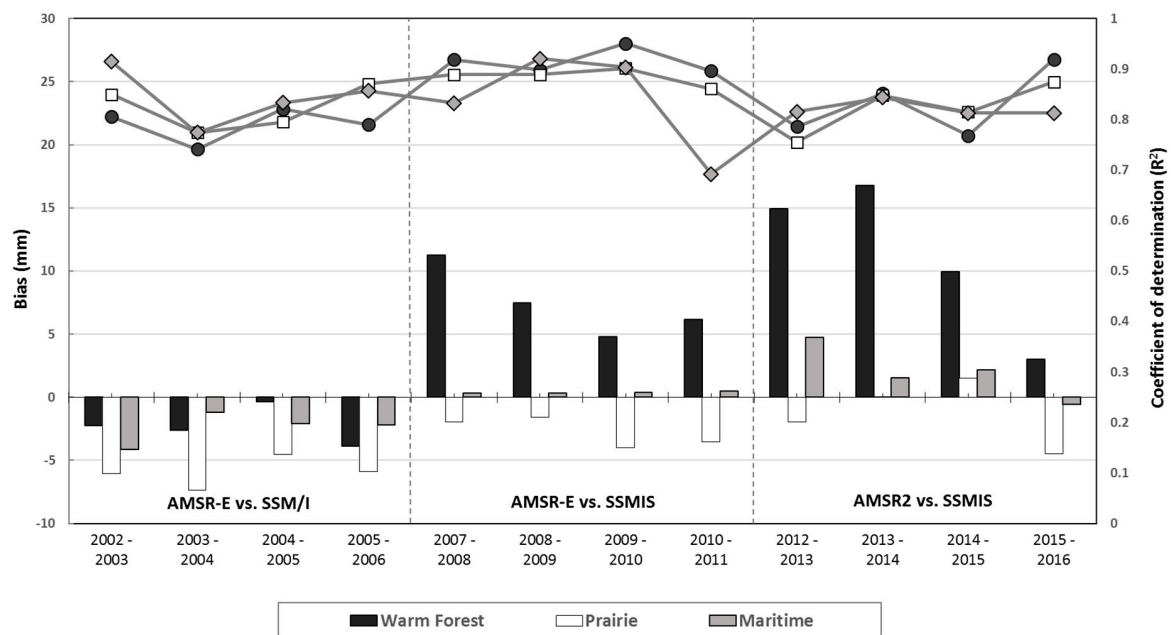


Figure 3. Yearly biases (bars) and R^2 (points) of AMSR-E and AMSR2 with SSMIS according to three snow classification.

Figure 3 shows the yearly averaged biases and R^2 values of SSM/I and SSMIS with AMSR-E SWE for the three snow classes. The comparison is divided between two periods (2002 to 2005 (SSM/I vs. AMSR-E) and 2007 to 2010 (SSMIS vs. AMSR-E)). The figure highlights that there are notable SWE bias differences between SSM/I and SSMIS sensors in the two periods. During the 2002–2005 winter seasons, all snow classes have negative biases, ranging from -1.25 to -7.57 mm. The patterns indicate that the SSM/I sensor usually overestimates SWE compared to AMSR-E. The average biases are -3.22 , -6.41 , and -2.73 mm for the Warm forest, Prairie, and Maritime classes, respectively. During the 2007–2010 winter seasons, the biases have a clearly different behavior based on snow class. The yearly biases of SSMIS in the Prairie class have similar negative patterns to SSM/I and the average biases in the Maritime class are close to 0 (0.68 mm). However, the Warm forest class has large SSMIS-AMSR-E

biases, ranging from 5.21 to 11.47 mm for the four winter seasons, which is notably different than the SSM/I-AMSR-E SWE bias in the Warm forest class.

Figure 4 shows boxplots between SSM/I and SSMIS SWE for a range of AMSR-E SWE intervals. The SSM/I sensor overestimates SWE values compared to SSMIS SWE in the Warm forest class over all AMSR-E SWE intervals. However, the Prairie class shows different patterns according to the magnitude of AMSR-E SWE. SSMIS SWE values are generally higher than SSM/I SWE for the high AMSR-E SWE intervals (>60 cm), while the SSM/I SWE values are higher than SSMIS SWE for the low intervals (0–20, 20–40, and 40–60 cm). The Maritime class has a similar pattern as the Prairie class, where SSM/I overestimates SWE values compared to SSMIS for low AMSR-E SWE ranges. However, the SSMIS SWE is slightly higher than SSM/I SWE for the highest interval (60–80 cm). The SSM/I and SSMIS SWE differences between low and high SWE may be attributable to SWE retrieval uncertainty related to deep snow. SWE retrieval errors generally increase during the snow accumulation period with developing deep snow packs [11].

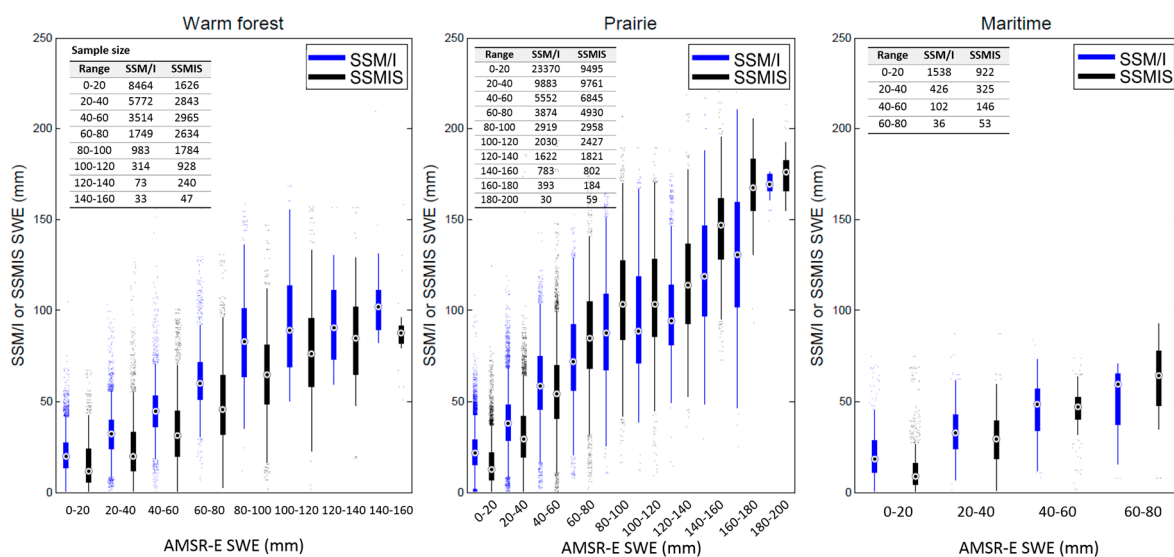


Figure 4. Boxplots of SSM/I and SSMIS SWE for different bins of AMSR-E SWE in three snow classes.

The differences between SSM/I and SSMIS SWE for snow classes, especially in the Warm forest class, are probably due to the difference in the interpolation methods for Tb between the F13 SSM/I and F17 SSMIS sensors [43,50]. Armstrong et al. [43] reported that the Backus-Gilbert interpolation method that had been used for the SSM/I sensors was not applied to the SSMIS EASE-Grid Tb, which were gridded using an inverse distance squared method. They mentioned that some larger differences, up to 10 K, were found in regions of steep Tb gradients due to the changes in geolocation. Considering the Chang SWE algorithm's equation, the difference in interpolation methods might influence the SWE difference between SSM/I and SSMIS. They also noted that the F17 SSMIS's source data version (Remote Sensing Systems Version 7, RSS V7) was different with that of F13 SSM/I (RRS V4). Brodzik [50] recommended that, unlike SSM/I Tb (V4), different coefficients should be used to retrieve SWE using the F17 SSMIS Tb (V7) inputs. The SSMIS Tb was already cross-calibrated with SSM/I as well as AMSR-E, providing inter-consistency of Tb from the sensors [43]. Considering our results, even though the satellite microwave Tb data were calibrated using previous and concurrent sensors, different Tb interpolation methods between a satellite sensor and its predecessor could lead to errors in Tb-derived hydrological variables, including SWE. These interpolation effects may vary according to regional characteristics. Overall, the results suggest that SSM/I and SSMIS SWE data users should be cautious using long-term SSM/I and SSMIS SWE data to draw conclusions based on temporal characteristics, especially in forested regions.

5.2. Comparison of AMSR-E and AMSR2 SWE with SSMIS SWE

Consistency between AMSR-E (2007 to 2010) and AMSR2 (2012 to 2015) SWE was evaluated for the three snow classes (Warm forest, Prairie, and Maritime), using SSMIS SWE as a baseline. Figure 2 shows that both AMSR-E and AMSR2 SWE have similar temporal variations with SSMIS SWE in most years. However, there are differences in the AMSR-E and AMSR2 SWE biases between the Warm forest and Prairie classes. Both AMSR-E and AMSR2 generally overestimate SWE values compared to SSMIS for the Warm forest, while they are slightly lower than SSMIS in the Prairie. These results are confirmed by yearly biases in Figure 3. The AMSR-E and AMSR2 SWE data have positive biases in the Warm forest class over the entire eight-year period, but have negative biases in the Prairie class in most years.

Based on yearly metrics (R^2 and bias), consistency between AMSR-E and AMSR2 SWE estimates are assessed using SSMIS SWE as a bridge dataset (Figure 3). When compared to SSMIS, AMSR-E has higher average R^2 values (0.92, 0.88, and 0.84) than AMSR2 SWE (0.83, 0.82, and 0.82) for the Warm forest, Prairie, and Maritime classes, respectively (Table 1). The AMSR2 sensor overestimates SWE values slightly more than AMSR-E in the Warm forest. The mean biases of AMSR2 (average: 11.16 mm) are higher than that of AMSR-E (average: 7.42 mm), as shown in Table 1. For the Prairie and Maritime classes, both sensors have relatively lower biases, within ± 5 mm (Figure 3). The yearly mean bias differences between AMSR2 and AMSR-E are 3.74, 1.54, and 1.60 mm for Warm forest, Prairie, and Maritime, respectively. The results indicate that SWE differences between AMSR2 and AMSR-E are generally less than the differences between SSM/I and SSMIS. Armstrong and Brodzik [29] found a 5 K difference in the $(Tb_{H19GHz} - Tb_{H37GHz})$ term between SMMR and SSM/I sensors over Northern Hemisphere. When applying to the Chang algorithm in Equation (1), the 5 K difference converts to approximately 24 mm of SWE, which is higher than mean-bias of AMSR-E and AMSR2 SWE.

Table 1. Mean biases and coefficient of determination (R^2) of AMSR-E/2 SWE relative to SSM/I & SSMIS SWE by year for different snow classes.

| Snow Class | | Bias (mm) | | | R^2 | | |
|----------------|--------------|--------------|--------------|--------------|-------------|-------------|-------------|
| | | Warm Forest | Prairie | Maritime | Warm Forest | Prairie | Maritime |
| AMSR-E & SSM/I | 2003 | −2.23 | −6.06 | −4.12 | 0.81 | 0.85 | 0.91 |
| | 2004 | −2.61 | −7.35 | −1.22 | 0.74 | 0.77 | 0.77 |
| | 2005 | −0.37 | −4.51 | −2.11 | 0.82 | 0.80 | 0.83 |
| | 2006 | −3.85 | −5.88 | −2.17 | 0.79 | 0.87 | 0.86 |
| | Aver. | −2.26 | −5.95 | −2.41 | 0.79 | 0.82 | 0.84 |
| AMSR-E & SSMIS | 2008 | 11.24 | −1.94 | 0.31 | 0.92 | 0.89 | 0.83 |
| | 2009 | 7.48 | −1.60 | 0.31 | 0.90 | 0.89 | 0.92 |
| | 2010 | 4.82 | −3.99 | 0.36 | 0.95 | 0.90 | 0.90 |
| | 2011 | 6.14 | −3.51 | 0.47 | 0.90 | 0.86 | 0.69 |
| | Aver. | 7.42 | −2.76 | 0.36 | 0.92 | 0.88 | 0.84 |
| AMSR2 & SSMIS | 2013 | 14.94 | −1.94 | 4.73 | 0.79 | 0.76 | 0.82 |
| | 2014 | 16.78 | 0.00 | 1.55 | 0.85 | 0.85 | 0.84 |
| | 2015 | 9.93 | 1.50 | 2.15 | 0.77 | 0.81 | 0.81 |
| | 2016 | 3.02 | −4.46 | −0.59 | 0.92 | 0.87 | 0.81 |
| | Aver. | 11.16 | −1.22 | 1.96 | 0.83 | 0.82 | 0.82 |

A final comparison was conducted in order to discern differences between AMSR-E and AMSR2 SWE based on the SSMIS SWE magnitude, and according to snow classification (Figure 5). The Warm Forest class generally has similar median values for AMSR-E and AMSR2 SWE except for the highest SSMIS SWE intervals (120–160 mm). For the Prairie class, there is little difference between AMSR-E and AMSR2 SWE for low and moderate SSMIS SWE ranges. However, the AMSR2 sensor overestimates SWE values compared to AMSR-E for the highest SWE ranges (140–200 mm). In the Maritime class, AMSR2 has higher SWE than AMSR-E SWE over the entire SSMIS SWE range, even though the

sample size for the Maritime class is much smaller than those of the Warm Forest and Prairie classes. Compared to Figure 4, the AMSR-E and AMSR2 sensors have more consistent SWE retrievals than SSM/I versus SSMIS, even though they have some differences at high SWE ranges. In conclusion, AMSR-E and AMSR2 SWE are relatively more consistent than SSM/I and SSMIS SWE based on the boxplots as well as time series and yearly statistics.

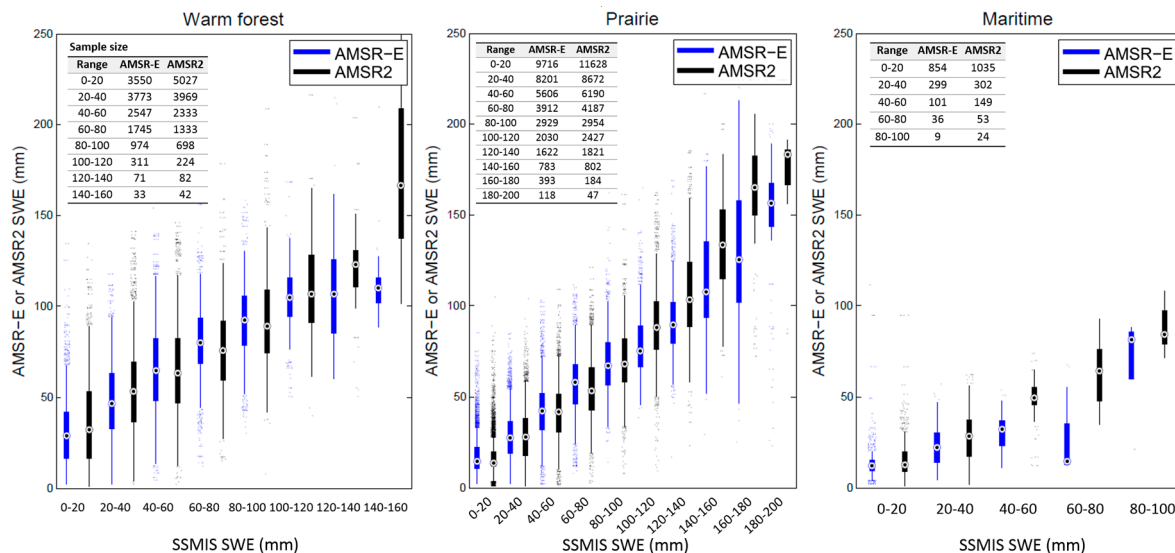


Figure 5. Boxplots of AMSR-E and AMSR2 SWE for different bins of AMSR-E SWE in three snow classes.

5.3. Spatial Bias Comparison between AMSR-E and AMSR2 with SSMIS SWE

Figure 6 depicts the spatial bias maps for AMSR-E and AMSR2 relative to SSMIS SWE over the 1176 watersheds in the study region. Positive biases (red color) indicate that AMSR-E/2 reports higher SWE values relative to SSMIS and negative biases (blue color) indicate that SSMIS has higher SWE values relative to AMSR-E/2. For the AMSR-E bias maps, there are negative biases in the northwest area and positive biases in the northeast area, while there are smaller biases over the middle and south part of the study regions. The bias patterns are consistent for all four years from 2007 to 2010 (Figure 6a). The AMSR2 maps also show generally similar spatial patterns with AMSR-E. The similarity of spatial patterns between AMSR-E and AMSR2 is confirmed by the metrics (see also Table 1). However, there are visible differences between the AMSR-E and AMSR2 bias maps in some parts of the study area (Figure 6). Especially in the northwest areas, the magnitude of AMSR2 SWE estimates is much larger than SSMIS, whereas this bias is much smaller between AMSR-E and SSMIS. This difference may be related to different climate conditions between the two analysis periods that resulted in large snow magnitudes from 2011 to 2015. Snow magnitude is well known as one of the error sources of satellite-based SWE [51–53]. To remove underlying climate effects, we obtained the normalized SWE bias maps for AMSR2 and AMSR-E using Equation (7). The spatial patterns of normalized SWE bias anomaly are very similar for AMSR2 and AMSR-E over the entire study area (Figure 7).

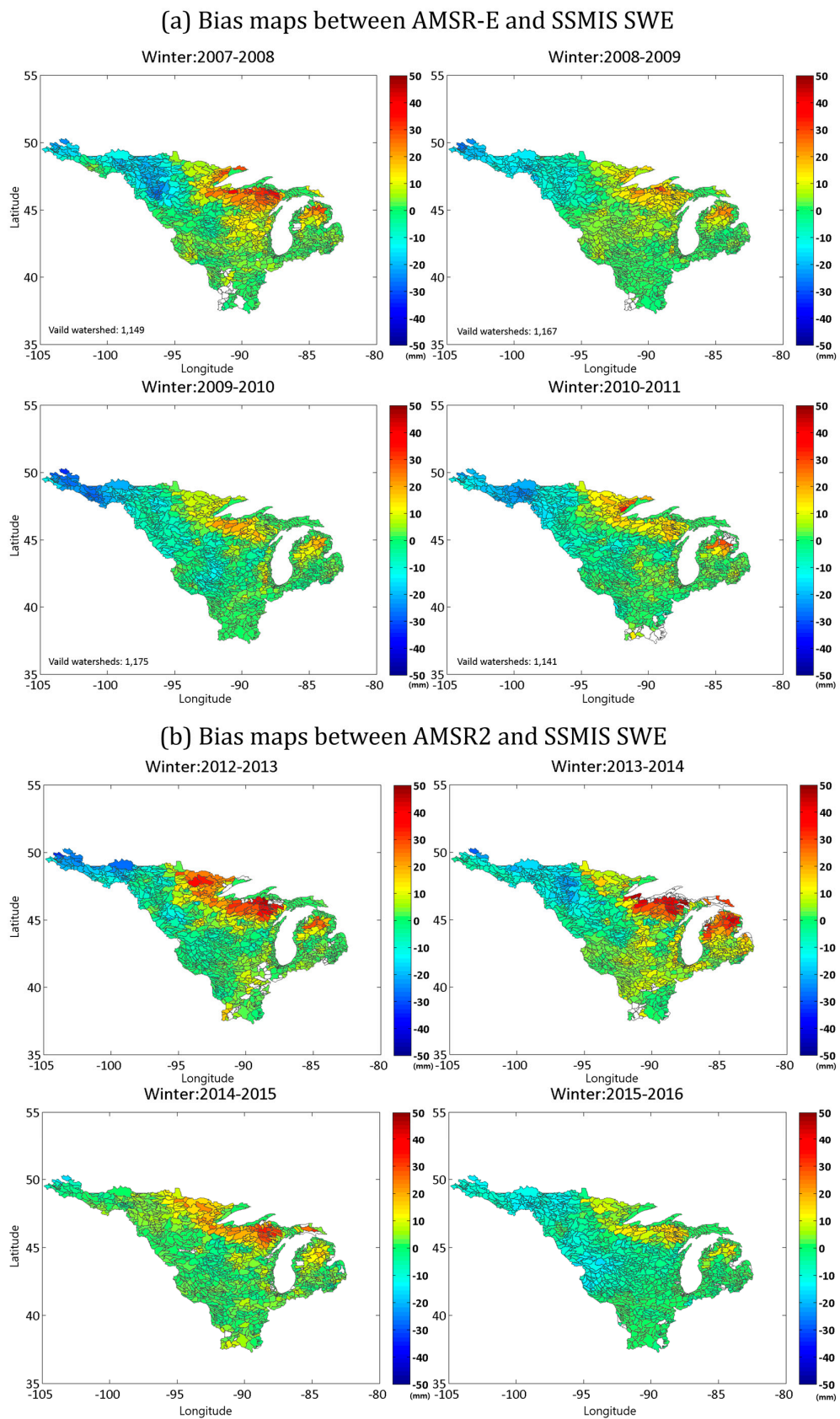


Figure 6. (a) Bias maps between AMSR-E (2007 to 2011) and (b) AMSR2 (2012 to 2016) SWE relative to SSMIS SWE in winter season (1 November–30 April).

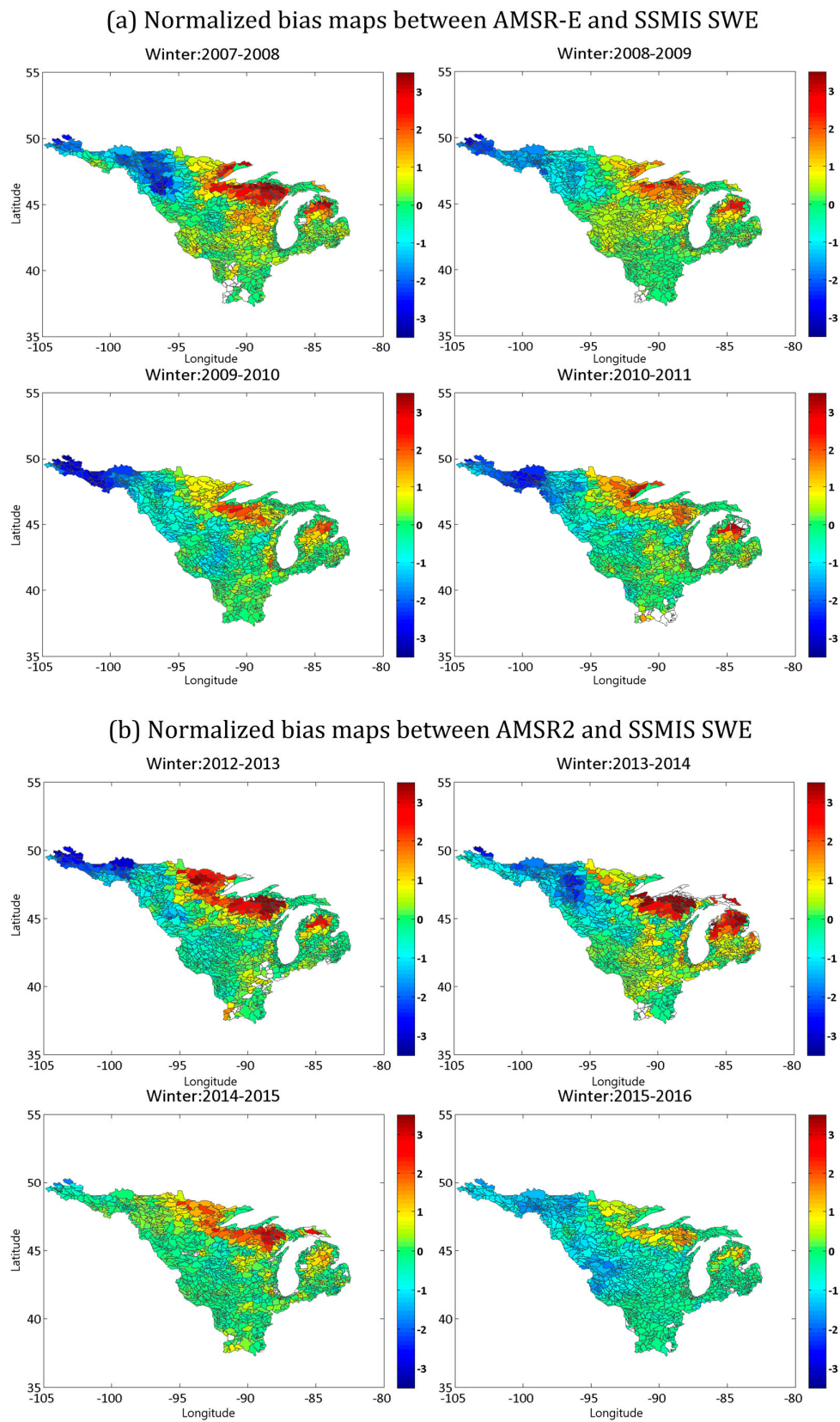


Figure 7. (a) Normalized bias maps between AMSR-E (2007 to 2011) and (b) AMSR2 (2012 to 2016) SWE relative to SSMIS SWE in winter season (1 November–30 April).

The AMSR2 maps show very similar spatial patterns across years, with higher positive biases in Warm forest area in Figure 6b. The spatial patterns may be closely related to regional characteristics (such as elevation, forest effects and latitude). The negative biases in the northwest area may partly correlate with the high elevation and high latitude. The results may be supported by the findings from Lee et al. [53], which showed that AMSR-E and AMSR2 snow depth biases increased by about 10 cm when elevation was changed from about 250 to 750 m. On the contrary, the lower biases in the middle and southern part could reflect the flat and nonforested surface features that are relatively ideal for microwave SWE retrievals [30,54].

The larger positive biases are clearly evident in the northeast areas, where the Warm forest class is dominant (Figure 1). These results are likely due to the difference between the retrieval algorithms' approach to capturing forest effects. Unlike the AMSR-E and AMSR2 algorithms, the Chang algorithm used for SSM/I and SSMIS does not account for forest fraction. As pointed out in earlier studies, the effects of canopy emission and scattering in forest areas could cause underestimation of microwave SWE [11,13,45,55]. The use of forest fraction to characterize the land surface in retrieval algorithms leads to significant quantitative differences in SWE estimates. Foster et al. [11] showed that underestimated SSM/I SWE estimates from the Chang algorithm were partly improved when the algorithm was modified to use forest fraction.

AMSR2 biases are spatially similar to AMSR-E biases, based on the normalized SWE maps. Although there are modest year-to-year differences in the bias patterns, the sensors show sufficient spatial consistency in sign and magnitude to treat the AMSR2 record as a continuation of AMSR-E. Regardless, approaches to remove systematic biases between instruments should be considered when application studies are sensitive to the magnitude of SWE bias (e.g., flood forecasting, climate trend analysis).

6. Conclusions

In this study, we evaluated consistencies in SWE estimated from different generations of similar passive microwave satellite sensors, using other satellite SWE data for temporal continuity. F13 SSM/I-F17 SSMIS was evaluated using AMSR-E and AMSR-E-AMSR2 SWE was examined using SSMIS for 1176 watersheds over the North Central U.S., according to three snow classifications (Warm forest, Prairie, and Maritime). There are notable bias differences between SSM/I and SSMIS-estimated SWE in the Warm forest class based on time series comparisons and yearly mean bias. It is likely that two SWE estimates are influenced by the difference interpolation methods for Tb between the F13 SSM/I and F17 SSMIS sensors. AMSR2 and AMSR-E satellite-based SWE retrievals have temporally reasonable agreement when compared to SSMIS SWE estimates. The SWE differences between AMSR2-E and AMSR2 are generally less than the differences between SSM/I and SSMIS SWE based on yearly metrics. The spatial bias patterns, normalized to SWE magnitude and variability, show good agreement between AMSR2 and AMSR-E SWE. The slight differences in SWE magnitudes may be partially due to sampling error from different climate conditions between two periods or systematic errors between the different instruments that could be related to ongoing calibration of AMSR2 Tb, although the basic characteristics of two sensors are quite similar [32].

Overall, careful consideration is required when using long-term SSM/I and SSMIS SWE data records by combining historical microwave sensors onboard the DMSP platform series, especially in SWE application studies such as snowmelt flood forecasting. Similarities in spatial patterns as well as metrics (bias and R^2) for AMSR2 and AMSR-E SWE suggest that the AMSR2 and AMSR-E combination provides a valuable source for a continuous microwave SWE estimates. Future research on this topic will enhance continuity of historical satellite-based SWE estimates and allow for continuous SWE estimates to be used for snowmelt flood-forecasting applications in areas such as the Red River of the North basin, where severe flood events have historically occurred.

Acknowledgments: This work was supported by a NASA Applied Water Resources Science Division grant (NNX15AC47G). Eunsang Cho was funded by the University of New Hampshire, College of Engineering Physical Science Graduate Fellowship in 2015–2016. We are grateful to all who contributed to the data sets used in this study. The authors also wish to thank the three anonymous reviewers for their useful comments.

Author Contributions: Eunsang Cho and Jennifer M. Jacobs conceived and designed the research. Eunsang Cho and Samuel E. Tuttle analyzed the data and Jennifer M. Jacobs gave comments and interpretations of the results. Eunsang Cho wrote the original manuscript, and Samuel E. Tuttle and Jennifer M. Jacobs edited this manuscript. All authors read and approved the submitted draft of the manuscript.

Conflicts of Interest: The authors declare no conflict of interest.

References

1. Doesken, N.J.; Judson, A. *The Snow Booklet: A Guide to the Science, Climatology, and Measurement of Snow in the United States*; Colorado State University Publications & Printing: Fort Collins, CO, USA, 1997.
2. Stocker, T. *Climate Change 2013: The Physical Science Basis: Working Group I Contribution to the Fifth Assessment Report of the Intergovernmental Panel on Climate Change*; Cambridge University Press: Cambridge, UK; New York, NY, USA, 2014.
3. Mankin, J.S.; Viviroli, D.; Singh, D.; Hoekstra, A.Y.; Diffenbaugh, N.S. The potential for snow to supply human water demand in the present and future. *Environ. Res. Lett.* **2015**, *10*, 114016. [[CrossRef](#)]
4. Berghuijs, W.R.; Woods, R.A.; Hutton, C.J.; Sivapalan, M. Dominant flood generating mechanisms across the United States. *Geophys. Res. Lett.* **2016**, *43*, 4382–4390. [[CrossRef](#)]
5. Miller, J.E.; Frink, D.L. *Changes in Flood Response of the Red River of the North Basin, North Dakota-Minnesota*; United States Government Printing Office: Washington, DC, USA, 1984.
6. Zhao, Q.; Liu, Z.; Ye, B.; Qin, Y.; Wei, Z.; Fang, S. A snowmelt runoff forecasting model coupling WRF and DHSVM. *Hydrol. Earth Syst. Sci.* **2009**, *13*, 1897–1906. [[CrossRef](#)]
7. Vuyovich, C.; Jacobs, J.M. Snowpack and runoff generation using AMSR-E passive microwave observations in the Upper Helmand Watershed, Afghanistan. *Remote Sens. Environ.* **2011**, *115*, 3313–3321. [[CrossRef](#)]
8. Marks, D.; Kimball, J.; Tingey, D.; Link, T. The sensitivity of snowmelt processes to climate conditions and forest cover during rain-on-snow: A case study of the 1996 Pacific Northwest flood. *Hydrol. Process.* **1998**, *12*, 1569–1587. [[CrossRef](#)]
9. Armstrong, R.; Brodzik, M. An earth-gridded SSM/I data set for cryospheric studies and global change monitoring. *Adv. Space Res.* **1995**, *16*, 155–163. [[CrossRef](#)]
10. Derksen, C.; Walker, A.E. Identification of systematic bias in the cross-platform (SMMR and SSM/I) EASE-grid brightness temperature time series. *IEEE Trans. Geosci. Remote Sens.* **2003**, *41*, 910–915. [[CrossRef](#)]
11. Foster, J.L.; Sun, C.; Walker, J.P.; Kelly, R.; Chang, A.; Dong, J.; Powell, H. Quantifying the uncertainty in passive microwave snow water equivalent observations. *Remote Sens. Environ.* **2005**, *94*, 187–203. [[CrossRef](#)]
12. Takala, M.; Luojus, K.; Pulliainen, J.; Derksen, C.; Lemmetyinen, J.; Kärnä, J.-P.; Koskinen, J.; Bojkov, B. Estimating northern hemisphere snow water equivalent for climate research through assimilation of space-borne radiometer data and ground-based measurements. *Remote Sens. Environ.* **2011**, *115*, 3517–3529. [[CrossRef](#)]
13. Vuyovich, C.M.; Jacobs, J.M.; Daly, S.F. Comparison of passive microwave and modeled estimates of total watershed SWE in the continental United States. *Water Resour. Res.* **2014**, *50*, 9088–9102. [[CrossRef](#)]
14. Jackson, T.J. Soil moisture estimation using special satellite microwave/imager satellite data over a grassland region. *Water Resour. Res.* **1997**, *33*, 1475–1484. [[CrossRef](#)]
15. Paloscia, S.; Macelloni, G.; Santi, E.; Koike, T. A multifrequency algorithm for the retrieval of soil moisture on a large scale using microwave data from SMMR and SSM/I satellites. *IEEE Trans. Geosci. Remote Sens.* **2001**, *39*, 1655–1661. [[CrossRef](#)]
16. Ramage, J.M.; Isacks, B.L. Interannual variations of snowmelt and refreeze timing on southeast-Alaskan icefields, USA. *J. Glaciol.* **2003**, *49*, 102–116. [[CrossRef](#)]
17. Ramage, J.; McKenney, R.; Thorson, B.; Maltais, P.; Kopczynski, S. Relationship between passive microwave-derived snowmelt and surface-measured discharge, Wheaton River, Yukon Territory, Canada. *Hydrol. Process.* **2006**, *20*, 689–704. [[CrossRef](#)]

18. Tedesco, M.; Brodzik, M.; Armstrong, R.; Savoie, M.; Ramage, J. Pan arctic terrestrial snowmelt trends (1979–2008) from spaceborne passive microwave data and correlation with the Arctic Oscillation. *Geophys. Res. Lett.* **2009**, *36*, L21402. [[CrossRef](#)]
19. Takala, M.; Pulliainen, J.; Metsamäki, S.J.; Koskinen, J.T. Detection of snowmelt using spaceborne microwave radiometer data in Eurasia from 1979 to 2007. *IEEE Trans. Geosci. Remote Sens.* **2009**, *47*, 2996–3007. [[CrossRef](#)]
20. Comiso, J.C.; Cavalieri, D.J.; Parkinson, C.L.; Gloersen, P. Passive microwave algorithms for sea ice concentration: A comparison of two techniques. *Remote Sens. Environ.* **1997**, *60*, 357–384. [[CrossRef](#)]
21. Liu, A.; Cavalieri, D. On sea ice drift from the wavelet analysis of the Defense Meteorological Satellite Program (DMSP) Special Sensor Microwave Imager (SSM/I) data. *Int. J. Remote Sens.* **1998**, *19*, 1415–1423. [[CrossRef](#)]
22. Jin, R.; Li, X.; Che, T. A decision tree algorithm for surface soil freeze/thaw classification over China using SSM/I brightness temperature. *Remote Sens. Environ.* **2009**, *113*, 2651–2660. [[CrossRef](#)]
23. Kim, Y.; Kimball, J.S.; McDonald, K.C.; Glassy, J. Developing a global data record of daily landscape freeze/thaw status using satellite passive microwave remote sensing. *IEEE Trans. Geosci. Remote Sens.* **2011**, *49*, 949–960. [[CrossRef](#)]
24. Kelly, R.E.; Chang, A.T.; Tsang, L.; Foster, J.L. A prototype AMSR-E global snow area and snow depth algorithm. *IEEE Trans. Geosci. Remote Sens.* **2003**, *41*, 230–242. [[CrossRef](#)]
25. Kelly, R. The AMSR-E snow depth algorithm: Description and initial results. *J. Remote Sens. Soc. Jpn.* **2009**, *29*, 307–317.
26. Tedesco, M.; Narvekar, P.S. Assessment of the NASA AMSR-E SWE Product. *IEEE J. Sel. Top. Appl. Earth Observ. Remote Sens.* **2010**, *3*, 141–159. [[CrossRef](#)]
27. Kelly, R.E. *Status of AMSR2 Level-2 Products (Algorithm Ver. 1.00)—Snow Depth*; JAXA Earth Observation Research Center: Saitama, Japan, 2013.
28. Kelly, R.E. *Status of AMSR2 Level-2 Products (Algorithm Ver. 2.00)—8. Snow Depth*; JAXA Earth Observation Research Center: Saitama, Japan, 2015.
29. Armstrong, R.L.; Brodzik, M.J. Recent northern hemisphere snow extent: A comparison of data derived from visible and microwave satellite sensors. *Geophys. Res. Lett.* **2001**, *28*, 3673–3676. [[CrossRef](#)]
30. Derksen, C.; Walker, A.; LeDrew, E.; Goodison, B. Combining SMMR and SSM/I data for time series analysis of central North American snow water equivalent. *J. Hydrometeorol.* **2003**, *4*, 304–316. [[CrossRef](#)]
31. Cavalieri, D.J.; Parkinson, C.L.; DiGirolamo, N.; Ivanoff, A. Intersensor Calibration Between F13 SSMI and F17 SSMIS for Global Sea Ice Data Records. *IEEE Geosci. Remote Sens. Lett.* **2012**, *9*, 233–236. [[CrossRef](#)]
32. Okuyama, A.; Imaoka, K. Intercalibration of Advanced Microwave Scanning Radiometer-2 (AMSR2) Brightness Temperature. *IEEE Trans. Geosci. Remote Sens.* **2015**, *53*, 4568–4577. [[CrossRef](#)]
33. Meier, W.N.; Khalsa, S.J.S.; Savoie, M.H. Intersensor calibration between F-13 SSM/I and F-17 SSMIS near-real-time sea ice estimates. *IEEE Trans. Geosci. Remote Sens.* **2011**, *49*, 3343–3349. [[CrossRef](#)]
34. Stadnyk, T.; Dow, K.; Wazney, L.; Blais, E.-L. The 2011 flood event in the Red River Basin: Causes, assessment and damages. *Can. Water Resour. J.* **2016**, *41*, 65–73. [[CrossRef](#)]
35. Wazney, L.; Clark, S.P. The 2009 flood event in the Red River Basin: Causes, assessment and damages. *Can. Water Resour. J.* **2016**, *41*, 56–64. [[CrossRef](#)]
36. Tuttle, S.E.; Cho, E.; Restrepo, P.J.; Jia, X.; Vuyovich, C.M.; Cosh, M.H.; Jacobs, J.M. Remote Sensing of Drivers of Spring Snowmelt Flooding in the North Central U.S. In *Remote Sensing of Hydrological Extremes*; Lakshmi, V., Ed.; Springer International Publishing: Cham, Switzerland, 2017; pp. 21–45.
37. Hirsch, R.; Ryberg, K. Has the magnitude of floods across the USA changed with global CO₂ levels? *Hydrol. Sci. J.* **2012**, *57*, 1–9. [[CrossRef](#)]
38. Melesse, A.M. Spatiotemporal dynamics of land surface parameters in the Red River of the North Basin. *Phys. Chem. Earth Parts A/B/C* **2004**, *29*, 795–810. [[CrossRef](#)]
39. Sturm, M.; Taras, B.; Liston, G.E.; Derksen, C.; Jonas, T.; Lea, J. Estimating Snow Water Equivalent Using Snow Depth Data and Climate Classes. *J. Hydrometeorol.* **2010**, *11*, 1380–1394. [[CrossRef](#)]
40. Liston, G.; Sturm, M. A global snow-classification dataset for earth-system applications. Unpublished work, 2014.
41. Sturm, M.; Holmgren, J.; Liston, G.E. A seasonal snow cover classification system for local to global applications. *J. Clim.* **1995**, *8*, 1261–1283. [[CrossRef](#)]

42. Kunkee, D.B.; Poe, G.A.; Boucher, D.J.; Swadley, S.D.; Hong, Y.; Wessel, J.E.; Uliana, E.A. Design and Evaluation of the First Special Sensor Microwave Imager/Sounder. *IEEE Trans. Geosci. Remote Sens.* **2008**, *46*, 863–883. [[CrossRef](#)]
43. Armstrong, R.; Knowles, K.; Brodzik, M.; Hardman, M. *DMSP SSM/I-SSMIS Pathfinder Daily EASE-Grid Brightness Temperatures, Version 2*; NASA National Snow Ice Data Center Distributed Active Archive Center: Boulder, CO, USA, 1994; Updated 2016; Available online: http://nsidc.org/data/docs/daac/nsidc0032_ssmi_ease_tbs.gd.html (accessed on 5 May 2016).
44. Chang, A.; Foster, J.; Hall, D.K. Nimbus-7 SMMR derived global snow cover parameters. *Ann. Glaciol.* **1987**, *9*, 39–44. [[CrossRef](#)]
45. Chang, A.; Foster, J.; Hall, D.; Goodison, B.E.; Walker, A.E.; Metcalfe, J.; Harby, A. Snow parameters derived from microwave measurements during the BOREAS winter field campaign. *J. Geophys. Res. Atmos.* **1997**, *102*, 29663–29671. [[CrossRef](#)]
46. Derksen, C.; LeDrew, E.; Walker, A.; Goodison, B. Influence of sensor overpass time on passive microwave-derived snow cover parameters. *Remote Sens. Environ.* **2000**, *71*, 297–308. [[CrossRef](#)]
47. Imaoka, K.; Kachi, M.; Kasahara, M.; Ito, N.; Nakagawa, K.; Oki, T. Instrument performance and calibration of AMSR-E and AMSR2. *Int. Arch. Photogramm. Remote Sens.* **2010**, *38*, 13–18.
48. Tedesco, M.; Kelly, R.; Foster, J.; Chang, A. *AMSR-E/Aqua Daily L3 Global Snow Water Equivalent EASE-Grids V002*; NASA National Snow Ice Data Center Distributed Active Archive Center: Boulder, CO, USA, 2004.
49. Kelly, R.E.; University of Waterloo, Waterloo, ON, Canada. Personal communication, 2016.
50. Brodzik, M.J. F17 vs. F13 SWE Regression. Available online: <http://cires1.colorado.edu/~brodzik/F13-F17swe/> (accessed on 20 January 2017).
51. Dong, J.; Walker, J.P.; Houser, P.R. Factors affecting remotely sensed snow water equivalent uncertainty. *Remote Sens. Environ.* **2005**, *97*, 68–82. [[CrossRef](#)]
52. Kelly, R.E.J.; Chang, A.T.C. Development of a passive microwave global snow depth retrieval algorithm for Special Sensor Microwave Imager (SSM/I) and Advanced Microwave Scanning Radiometer-EOS (AMSR-E) data. *Radio Sci.* **2003**, *38*. [[CrossRef](#)]
53. Lee, Y.-K.; Kongoli, C.; Key, J. An In-Depth Evaluation of Heritage Algorithms for Snow Cover and Snow Depth Using AMSR-E and AMSR2 Measurements. *J. Atmos. Ocean. Technol.* **2015**, *32*, 2319–2336. [[CrossRef](#)]
54. Langlois, A.; Royer, A.; Dupont, F.; Roy, A.; Goita, K.; Picard, G. Improved Corrections of Forest Effects on Passive Microwave Satellite Remote Sensing of Snow Over Boreal and Subarctic Regions. *IEEE Trans. Geosci. Remote Sens.* **2011**, *49*, 3824–3837. [[CrossRef](#)]
55. Roy, A.; Royer, A.; Hall, R.J. Relationship between forest microwave transmissivity and structural parameters for the Canadian boreal forest. *IEEE Geosci. Remote Sens. Lett.* **2014**, *11*, 1802–1806. [[CrossRef](#)]



© 2017 by the authors. Licensee MDPI, Basel, Switzerland. This article is an open access article distributed under the terms and conditions of the Creative Commons Attribution (CC BY) license (<http://creativecommons.org/licenses/by/4.0/>).